

論文の内容の要旨

論文題目 Performance, Stability and Control of a VTOL Ducted Fan
(垂直離着陸ダクトドファンの安定性と性能に関する研究)

氏名 コルマン マイルス リチャード

Research Outline

Ducted fans are the only vertical takeoff and landing vehicles capable of efficient hover and cruise at equal power. This work reports on design, wind tunnel tests, and transition simulation of a high-efficiency ducted fan with cyclic pitch actuation designed to use equal power in hover and cruise. The rotor shroud is a ring wing designed for efficient cruise. Conventional duct leading edges are also tested in hover, and with a crosswind. The results of this research may be used to increase the cruise efficiency and pitch control authority of unmanned aerial vehicles while reducing design constraints imposed by the transition corridor.

In this work, the following hypotheses are tested:

- Airfoil section data may be used with vortex lattice codes to accurately predict the aerodynamic coefficients of a ring wing.
- Use of a ring wing as the rotor shroud of a ducted fan results in high lift to drag ratios and useful lift coefficients at low angle of attack in a near-axial flow flight condition.
- Use of cyclic pitch for moment control is adequate for stabilization in hover and cruise.

Abstract

The ducted fan is unique among VTOL vehicles in that it can cruise and hover efficiently at the hover power setting. A graph of ducted fan power required in cruise as a function of lift coefficient and L:D ratio is shown in Fig. 2.

Experimental wind tunnel data for a new ring wing (shown in Fig. 2) is presented. At a chord Reynolds number of 250,000, the biplane-cambered aspect ratio 3.1 ring wing has a lift to drag ratio greater than 12, developed at 4 degrees angle of attack. High lift to drag ratio is due to the biplane-cambered airfoil stack, shown in Fig. 3. Ring wing lift, drag and moment data are taken from 0 to 90 degrees of the angle of attack. The ring's minimum internal diameter is 600 mm.

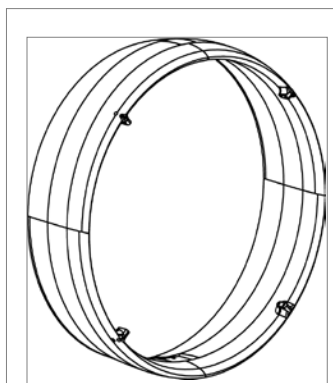


Figure 1: Perspective View of Ring Wing

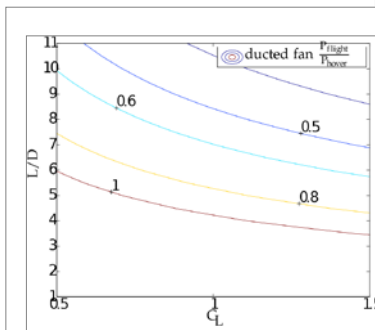


Figure 4: Power fraction of hover for cruising ducted fan as a function of lift coefficient and lift to drag ratio. Assumptions: 30% rotor offloading in hover and aspect ratio 3.

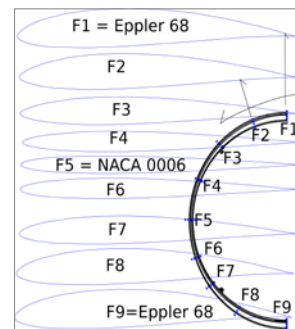


Figure 3: New Ring Wing Airfoil Stack

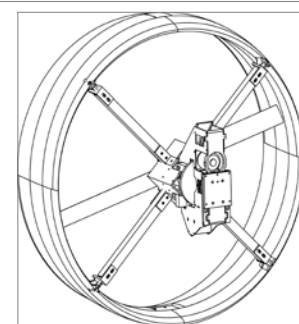


Figure 2: Ring Wing with Heli Fuselage and Rotor Blades

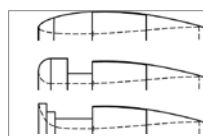


Figure 6: Cross-section detail of interchangeable lip. Top to bottom: airfoil, circular, trumpet.

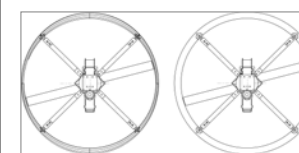


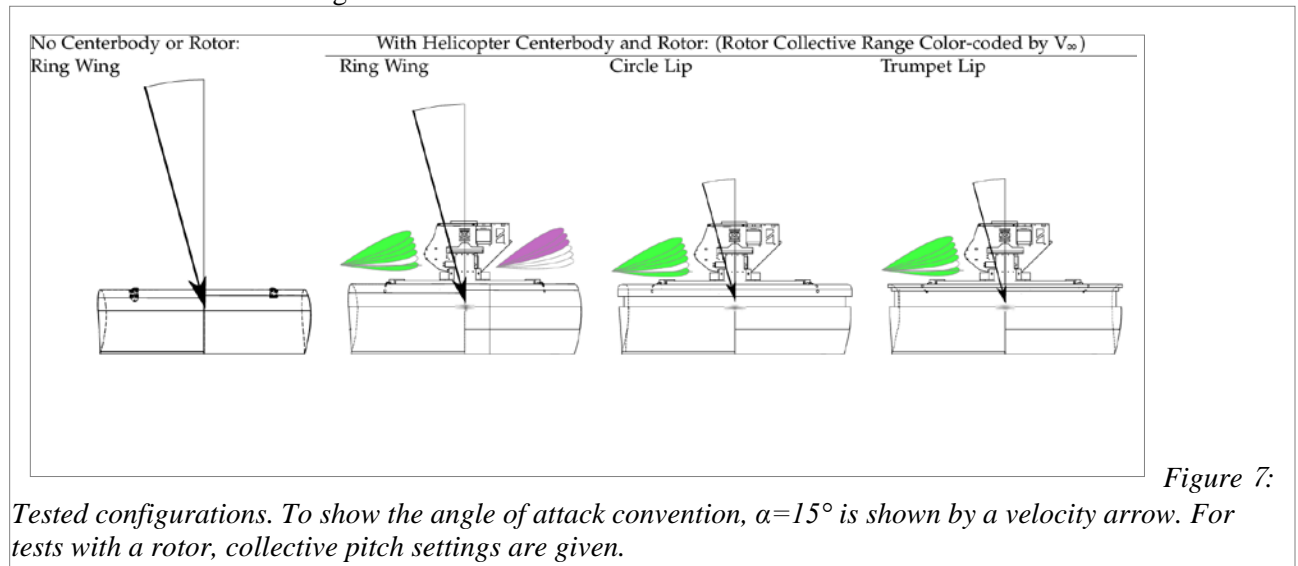
Figure 5: Front view of airfoil (l), and circular and trumpet lips (r), mounted on ducted fan as tested in wind tunnel

The ring wing in use as a duct is shown in Fig. 4. Untapered, untwisted NACA 0015 helicopter blades are used for the rotor. Force and moment data were taken for the ducted fan in hover, with and without a 10 m/s headwind, and in near axial-flow conditions at 15 m/s.

Thrust and power coefficients are presented for the no-headwind hover case, with three different duct lips, a circular lip, a trumpet lip, and the lip of the ring wing tested by itself. Front views of all duct lips are shown in Fig. 5. The interchangeable duct lips are shown in cross section in Fig. 6.

Ducted fan maximum test Reynolds number is 190,000. Rotor collective pitch settings from 0 to 25 degrees, and helicopter-type cyclic pitch settings from 0 to 7.5 degrees were tested. Ducted fan maximum lift to drag ratio with unfaired struts and centerbody was 4. This value could easily be improved to 8 or higher by fairing the struts and centerbody. Cyclic pitch response was found to be linear below blade stall. Large moments were produced in hover and cruise, sufficient to stabilize the vehicle and provide maneuvering capability.

Large control moments available from cyclic pitch in hover and near-axial flow conditions may enable dynamic transitions from hover to cruise. The simple, accurate models developed for power-off shroud aerodynamic performance enable UAV design for longer loiter and more efficient cruise flight.



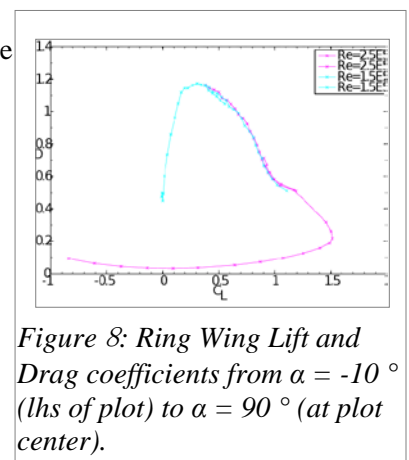
Wind Tunnel Test Overview

Configurations tested in the wind tunnel are shown in Fig. 7. The test range covers crosswind and axial flow for the ring wing and ring wing with rotor and the different duct lips. For the ring wing, intermediate angles of attack are also checked.

Results from Wind Tunnel Testing

A ducted fan with axial asymmetry has been tested for hover performance with a variety of duct lips at low Reynolds numbers. The experimental results provide the first published force and moment data for cyclic pitch-actuated ducts with axial asymmetry.

Aspect ratio 3.1 ring wing polars were accurately predicted using the AVL vortex lattice code on a wing with circumferentially varying camber. Wind tunnel lift and drag coefficients for the tested ring wing are shown in Fig. 8. Lift to drag ratios greater than 12 occur at a C_L range of 1-1.2, near 4 degree angle of attack. Calculated polar and span efficiency factor is compared with the experimental



ring wing lift polar in Fig. 9. It can be seen that section methods provide a good trust region for lift coefficient estimation. The C_{D0} offset for the AVL drag figure is a circumferential average of section drag coefficients at zero angle of attack, multiplied by pi.

Solidity-weighted thrust coefficient versus power coefficient for no-crosswind hover are presented in Fig. 12, with comparison data from NACA TN 626. It can be seen that the trumpet and circular rotor shrouds increase efficiency beyond the induced power theoretical limit, for the trumpet and circular duct lips. In addition, at constant solidity, useful C_T range is increased by the use of a duct.

In crosswinds, rotor offloading for the trumpet and circular duct lips is reduced, and pitching moments are increased relative to the airfoil duct lip.

Total recorded moment due to cyclic pitch (changing the angle of attack of the rotor blades as they rotate) is shown in Figs. 10 and 11. Based on hover and crosswind hover wind tunnel tests of cyclic pitch actuation, cyclic pitch actuation is adequate for moment control, even with crosswinds of 0.14 times the blade tip speed.

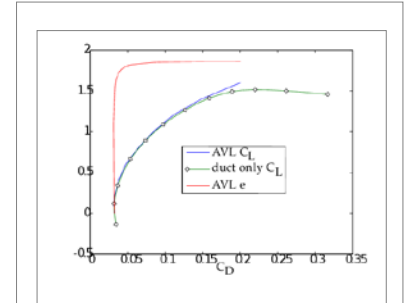


Figure 9: Athena Vortex Lattice polar agrees with experiment; span efficiency factor ϵ reaches 1.86 (based on projected area)

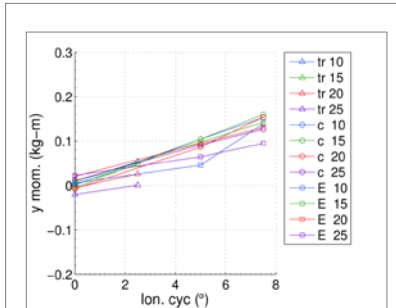


Figure 10: Ducted fan hover pitching moment as a function of applied cyclic pitch.

Generated pitching moments are presented for hover and hover with crosswind. 'tr' means trumpet lip, 'c' means circle lip, and 'E' means airfoil lip. Lip name is followed by the collective pitch setting.

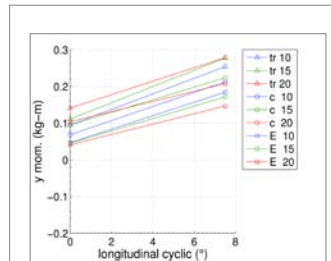


Figure 12: Crosswind hover pitching moment as a function of applied cyclic pitch. Cyclic pitch travel extends from -9 to +9 degrees, so the expected crosswind pitching moment can be countered.

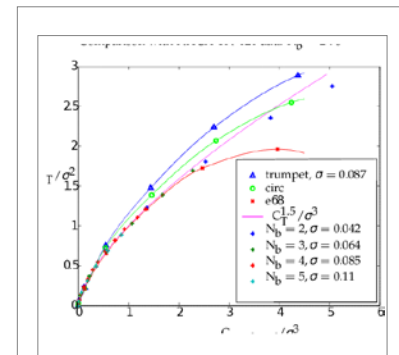


Figure 11: Solidity-weighted thrust coefficient versus solidity-weighted power coefficient. e68 is the ring wing with rotor and centerbody.

Conclusions from Longitudinal Simulation of Ducted Fan Flight

Cruise condition lift to drag for the ducted fan, shown in Fig. 13, reaches a maximum of about 4 at the highest allowable angle of attack. This is due to the high bluff body drag of the tested configuration. Lift to drag ratios greater than 8 should be easily achievable by the use of faired struts and centerbody, instead of the square struts and centerbody shown in Fig. 4.

Open-loop rotor collective pitch doublet response is unstable, as shown in Fig. 14. The trimmed ducted fan ($x_{cg}=.25c$) position has an unstable phugoid mode. The collective pitch control offers direct control of airspeed. As seen in Fig. 15, the cyclic pitch control is an effective control for the duct attitude, and also offers immediate response in flight path angle. The cyclic doublet response shows undesirable coupling to the flight path velocity.

Discussion

This work has presented selected results from aerodynamic analysis and wind tunnel tests of a ducted fan. The duct was designed for efficient lift in a near axial flow condition. The design is limited to UAVs due to the need to vary fuselage horizon angle from 90 to 0 degree from hover to cruise.

The use of airfoil section data and vortex lattice codes for shroud design was validated with experimental data for a new ring wing. The ring wing has high efficiency in axial flow at low chord Reynolds numbers.

In hover, it is found that duct lips with small curvature give useful rotor offloading at helicopter thrust coefficients. Comparison of induced power to thrust show that the induced efficiency gain is equivalent to increased rotor area, but without the increased profile drag penalty. Airfoil-shaped duct lips do not offer offloading, but have lower crosswind pitching moment.

Experimental results show that large control moments can be obtained by cyclic pitch application in hover and cruise. Large control moments are useful for rapid transitions from hover to cruise and back. Such transitions might be used by UAVs, eliminating trim requirements in the separated flow fuselage angle of attack range.

It is shown in simulation that the control-input responses are coupled. Cyclic and collective pitch are effective controls in simulations using experimental wind tunnel data for the shrouds tested. Finally, the desired lift to drag ratio, while not achieved in tests, could be gained by strut and centerbody streamlining.

Summary

-A new, cruise-efficient shroud is shown to match predicted high efficiency in axial flow conditions. Increased loiter capability and range are predicted for ducted fans using shrouds of the type presented here.

-High moment generation capability was reported using cyclic pitching of the blades. If control responses are properly decoupled, control surfaces will no longer need to be sized for sustained flight in the transition region between cruise and hover flight, allowing further increases in aerodynamic and structural efficiency.

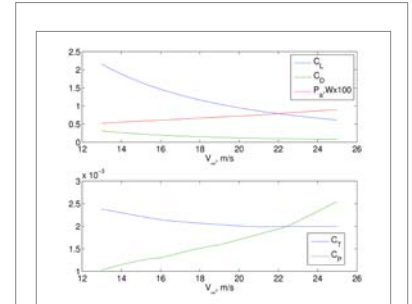


Figure 13: Lift and drag coefficients in the cruise condition based on simulation using wind tunnel data. In the upper plot, lift, drag and aerodynamic power in 100s of watts are plotted against freestream velocity. In the lower plot, thrust and power coefficient are plotted against freestream velocity.

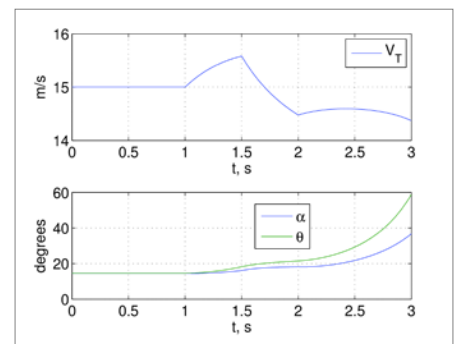


Figure 14: Collective doublet response

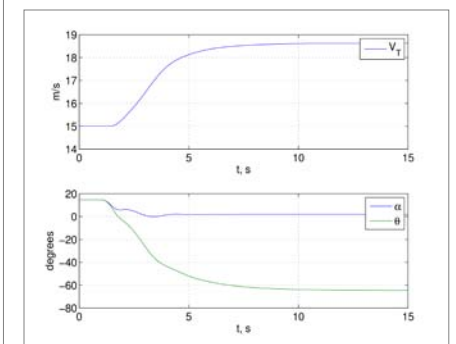


Figure 15: Cyclic doublet response